Contrasting effect of La substitution on the magnetic moment direction in the Kondo semiconductors CeT_2Al_{10} (T=Ru,Os)

D. T. Adroja,[1,2,*] A. D. Hillier,[1] C. Ritter,[3] A. Bhattacharyya,[1,2] D. D. Khalyavin,[1] A. M. Strydom,[2,4] P. Peratheepan,[2,5] B. Fåk,[3] M. M. Koza,[3] J. Kawabata,[6] Y. Yamada,[6] Y. Okada,[6] Y. Muro,[7] T. Takabatake,[6] and J. W. Taylor[1]

[1]*ISIS Facility, Rutherford Appleton Laboratory, Chilton, Didcot, Oxon, OX11 0QX, United Kingdom*

[2]*Highly Correlated Matter Research Group, Physics Department, University of Johannesburg, Auckland Park 2006, South Africa*

[3]*Institut Laue-Langevin, BP 156, 6 Rue Jules Horowitz 38042, Grenoble Cedex, France*

[4]*Institute for Solid State Physics, Vienna University of Technology, Wiedner Hauptstrasse 8-10/138, 1040 Vienna, Austria*

[5]*Department of Physics, Eastern University, Vantharumoolai, Chenkalady 30350, Sri Lanka*

[6]*Department of Quantum Matter, ADSM and IAMR, Hiroshima University, Higashi-Hiroshima 739-8530, Japan*

[7]*Faculty of Engineering, Toyama Prefectural University, Toyama 939-8530, Japan*

(Received 29 January 2015; revised manuscript received 3 August 2015; published 14 September 2015)

The opening of a spin gap in the orthorhombic compounds CeT_2Al_{10} (T = Ru and Os) is followed by antiferromagnetic ordering at T_N = 27 and 28.5 K, respectively, with a small ordered moment (0.29–0.34 μ_B) along the c axis, which is not an easy axis of the crystal field (CEF). In order to investigate how the moment direction and the spin gap energy change with La doping in $Ce_{1-x}La_xT_2Al_{10}$ (T = Ru and Os) and also to understand the microscopic nature of the magnetic ground state, we here report on magnetic, transport, and thermal properties, neutron diffraction (ND), and inelastic neutron scattering (INS) investigations on these compounds. Our INS study reveals the persistence of spin gaps of 7 and 10 meV in the 10% La-doped T = Ru and Os compounds, respectively. More interestingly our ND study shows a very small ordered moment of 0.18 μ_B along the b axis in $Ce_{0.9}La_{0.1}Ru_2Al_{10}$, however a moment of 0.23 μ_B still along the c axis in $Ce_{0.9}La_{0.1}Os_2Al_{10}$. This contrasting behavior can be explained by a different degree of hybridization in $CeRu_2Al_{10}$ and $CeOs_2Al_{10}$, being stronger in the latter than in the former. Muon spin rotation (μSR) studies on $Ce_{1-x}La_xRu_2Al_{10}$ (x = 0, 0.3, 0.5, and 0.7), reveal the presence of coherent frequency oscillations indicating a long-range magnetically ordered ground state for x = 0 to 0.5, but an almost temperature independent Kubo-Toyabe response between 45 mK and 4 K for x = 0.7. We compare the results of the present investigations with those reported on the electron and hole doping in CeT_2Al_{10}.

DOI: 10.1103/PhysRevB.92.094425 PACS number(s): 71.27.+a, 75.30.Mb, 75.20.Hr, 25.40.Fq

I. INTRODUCTION

In recent years, the magnetic and transport properties of Ce-based ternary compounds of type CeT_2Al_{10} (T = Fe, Ru, and Os), which crystalline in the orthorhombic structure (space group No. 63 $Cmcm$) [1], have generated strong interest in both theoretical and experimental condensed matter physics [2–13]. The resistivity of $CeRu_2Al_{10}$ exhibits a sharp drop near 27 K resembling an insulator-metal transition [2]. A very similar phase transition, near 29 K, has been observed in $CeOs_2Al_{10}$ [8,14], but in this compound the susceptibility (along the a axis) exhibits a broad maximum near 45 K in contrast to a sharp drop at the phase transition (27 K) in $CeRu_2Al_{10}$ [8,15]. The broad maximum in the susceptibility and its strong anisotropic behavior in the paramagnetic state reveal the presence of strong hybridization between $4f$ and conduction electrons as well as strong single ion anisotropy arising from the crystal field potential [16,17]. The compound $CeFe_2Al_{10}$ exhibits Kondo insulating behavior with a transport-derived gap of 15 K [3], while an NMR study reveals a much larger value of the gap, namely 110 K [18].

Neutron diffraction (ND) studies of CeT_2Al_{10} (T = Ru and Os) reveal very small moments in the antiferromagnetically (AFM) ordered states, 0.34 and 0.29 μ_B, respectively, along the c axis, which is not the direction expected from the single ion crystal field (CEF) anisotropy [5,6,19]. As the single ion crystal field would prefer the moment along the a axis in both compounds, this indicates that the moment direction is governed by the anisotropic magnetic exchange and not by the CEF anisotropy. The inelastic neutron scattering (INS) studies at 4.5 K on the polycrystalline samples of CeT_2Al_{10} (T = Ru, Os, and Fe) reveal a clear sign of a spin-gap formation of 8, 11, and 12 meV, respectively [20–22]. Very recently INS investigations on single crystals of $CeRu_2Al_{10}$, $CeOs_2Al_{10}$, and $CeFe_2Al_{10}$ have been performed [20,21,23]. Well defined gapped spin waves are observed in $CeRu_2Al_{10}$ and $CeOs_2Al_{10}$ that can well be explained by anisotropic exchange interactions. Even in the paramagnetic state of $CeFe_2Al_{10}$ (no magnetic ordering observed down to 50 mK) the INS study reveals a dispersive gapped magnetic excitation having the same propagation vector k = (1,0,0) as observed in $CeRu_2Al_{10}$, suggesting that these magnetic excitations in the Kondo insulating state have some connection to the spin wave observed in the magnetically ordered state of CeT_2Al_{10} (T = Ru and Os) [20,21].

The studies of electron (Ir/Rh) and hole (Re) doping on the transition metal site in CeT_2Al_{10} (T = Ru and Os) [10,11,24] reveal the general trend that the hybridization between $4f$ electrons and conduction electrons increases with hole doping, while the Ce-$4f$ electrons become more localized with electron doping. On hole doping the spin gap and the AFM order with an anomalous direction of the magnetic moment (i.e., moment either along the c axis or b axis) not governed

*devashibhai.adroja@stfc.ac.uk

by the single ion crystal field anisotropy survive [6,24,25]. In contrast to this, electron doping destabilizes the spin gap formation and the AFM ordering becomes normal with moment directions along the a axis, e.g., governed by the single ion anisotropy, and larger values of the ordered state moment, $\approx 1\ \mu_B$ [26].

Kondo *et al.* [27] found that T_N is suppressed by the application of a magnetic field as well as by La substitution on the Ce site in $CeRu_2Al_{10}$. Considering these interesting observations found with electron- and hole-doped $CeRu_2Al_{10}$ and $CeOs_2Al_{10}$, it is timely to investigate the effect of chemical pressure (La or Y doping) on the Ce site in CeT_2Al_{10} (T = Ru and Os) using microscopic techniques such as ND, INS, and μSR measurements. We therefore present in this paper our results of such measurements on La-substituted $Ce_{1-x}La_xT_2Al_{10}$ (T = Ru and Os) to shed light on the nature of the phase transition and the ground state of the Ce ion in these compounds.

The effect of La and Y substitution on the parent compound $CeRu_2Al_{10}$ has been investigated before by three groups by studying magnetic and transport properties [28–30]. La (Y) has a bigger (smaller) ionic radius compared to Ce and hence La substitution expands the lattice corresponding to negative chemical pressure and Y substitution contracts the lattice corresponding to that to positive chemical pressure. The results are interesting and unexpected [28,29]. With increasing La concentration x in $Ce_{1-x}La_xRu_2Al_{10}$, the transition temperature is progressively shifting to lower temperature and vanishes near the critical composition $x_c \approx 0.7$ [30,31]. Surprisingly Y substitution leads as well to a decrease of T_N rather than to an increase as one would expect for positive chemical pressure, and disappears suddenly between $x = 0.4$ and 0.5 [31]. This behavior cannot be understood by a simple magnetic phase transition, suggesting that the change in the valence of Ce ion plays an important role in the mysterious phase transition [31,32].

From the single crystal susceptibility measurements Tanida *et al.* [33] have proposed that 10% La doping in $CeRu_2Al_{10}$ changes the direction of the ordered state moment from the c axis found in undoped system to the b axis, the hard axis of magnetization. Application of a pressure of 0.3 GPa changes the moment back to the c axis [33]. However, magnetic susceptibility data can only give indirect information on the ordered state moment direction and cannot give a direct measure of the value of the ordered state moment. The unanswered question remains what is happening to the spin gap formation and its energy scale as the direction of the ordered state moment of $Ce_{0.9}La_{0.1}Ru_2Al_{10}$ changes to the b axis from the c axis as in $CeRu_2Al_{10}$. In order to answer these questions we have carried out ND and INS measurements on $Ce_{0.9}La_{0.1}Ru_2Al_{10}$ as well as on $Ce_{0.9}La_{0.1}Os_2Al_{10}$. In order to gain further information on the microscopic change in the magnetism we have also performed muon spin rotation measurements on $Ce_{1-x}La_xRu_2Al_{10}$ ($x = 0$, 0.3, 0.5, and 0.7) alloys.

II. EXPERIMENTAL DETAILS

The polycrystalline samples of $Ce_{1-x}La_xRu_2Al_{10}$ (x = 0, 0.1, 0.3, 0.5, and 0.7), $Ce_{0.9}La_{0.1}Os_2Al_{10}$, $LaRu_2Al_{10}$, and $LaOs_2Al_{10}$ were prepared by argon arc melting of the stoichiometric constituents with the starting elements, Ce/La 99.9% (purity), Ru/Os 99.9%, and Al 99.999%. The samples were annealed at 800 °C for seven days in an evacuated quartz ampoule. The samples were characterized using powder x-ray diffraction or neutron diffraction (on D2B diffractometer at ILL, Grenoble) at 300 K and were found to be dominantly single phase (see Fig. 1). Magnetic susceptibility measurements were made using a Magnetic Property Measurement System (MPMS) superconducting quantum interference device (SQUID) magnetometer (Quantum Design). Electrical resistivity by the four probe method and heat capacity by the relaxation method were performed in a Quantum Design Physical Properties Measurement System (PPMS). The μSR experiments were carried out using the MUSR spectrometer in longitudinal geometry at the ISIS muon source, UK, and the details on the experimental technique can be found in [6,7]. The powdered samples were mounted onto a 99.995+% pure silver plate.

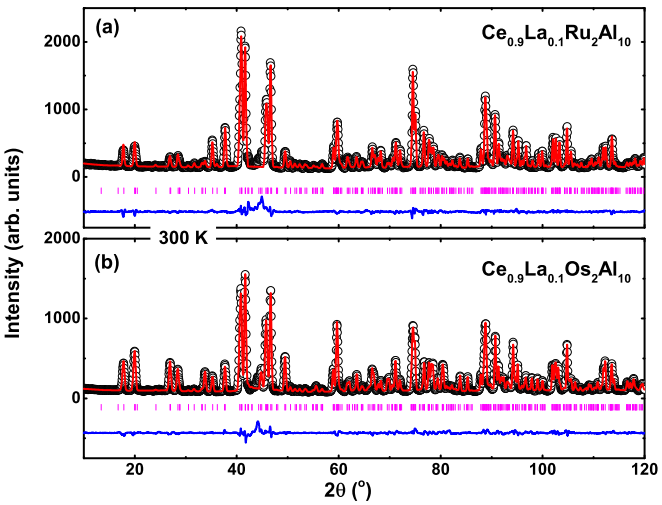

FIG. 1. (Color online) (a) and (b) Rietveld refinement of the neutron powder diffraction pattern of $Ce_{0.9}La_{0.1}T_2Al_{10}$ (T = Ru and Os) at 300 K collected using the D2B diffractometer with wavelength $\lambda = 1.594$ Å. The circle symbols (black) and solid line (red) represent the experimental and calculated intensities, respectively, and the line below (blue) is the difference between them. Tick marks indicate the positions of Bragg peaks in the $Cmcm$ space group.

The low-temperature ND measurements at 1.5 and 35 K on $Ce_{0.9}La_{0.1}Ru_2Al_{10}$ and $Ce_{0.9}La_{0.1}Os_2Al_{10}$ samples were performed using the high neutron flux D20 diffractometer at ILL, Grenoble, France, using constant wavelengths of 1.3 or 2.41 Å. The powder samples were mounted in a 10 mm diameter vanadium can, which was cooled down to 2 K using a standard He-4 cryostat. The program FULLPROF [35] was used for Rietveld refinements and group theoretical calculations were performed with the aid of the Sarah/ISOTROPY software [36,37].

The INS measurements between 2 and 35 K on $Ce_{0.9}La_{0.1}Ru_2Al_{10}$, $Ce_{0.9}La_{0.1}Os_2Al_{10}$, $CeRu_2Al_{10}$, $LaRu_2Al_{10}$, and $LaOs_2Al_{10}$ (15 g sample) were carried out using the MARI and MERLIN time-of-flight (TOF) chopper spectrometers at ISIS Facility, while measured

on $Ce_{0.9}La_{0.1}Ru_2Al_{10}$ and $LaRu_2Al_{10}$ additional data were collected on the IN4 TOF chopper spectrometer at ILL, Grenoble, France. On MARI/MERLIN the samples were wrapped in a thin Al foil and mounted inside a thin-walled cylindrical Al can, which was cooled down to 4.5 K inside a top-loading closed-cycle refrigerator (TCCR) with He-exchange gas around the samples. The measurements were performed with an incident neutron energy E_i of 25 meV (20 meV), with an elastic resolution (at zero energy transfer) of 1.1 meV (0.8 meV) (FWHM). On IN4 the samples were wrapped in a thin Al foil, which was cooled down to 2 K inside a standard He-4 cryostat with He-exchange gas around the samples. The measurements were performed with an incident neutron energy E_i of 16.9 meV, with an elastic resolution (at zero energy transfer) of 1.1 meV (FWHM).

III. RESULTS AND DISCUSSIONS

Bulk properties

To explain the overall bulk properties of the title compounds, we present here their magnetic susceptibility, electric resistivity, and specific heat data with emphasis on the magnetic phase transitions. Figures 2(a)–2(f) show the temperature dependent magnetic susceptibility, electrical resistivity, and heat capacity of $Ce_{0.9}La_{0.1}Ru_2Al_{10}$ and $Ce_{0.9}La_{0.1}Os_2Al_{10}$. The magnetic susceptibility $\chi(T)$ of $Ce_{0.9}La_{0.1}Ru_2Al_{10}$ exhibits a clear peak near 23.0 K, which is due to an AFM ordering of Ce moments. On the other hand, $\chi(T)$ of $Ce_{0.9}La_{0.1}Os_2Al_{10}$ exhibits a broad maximum near 40 K and

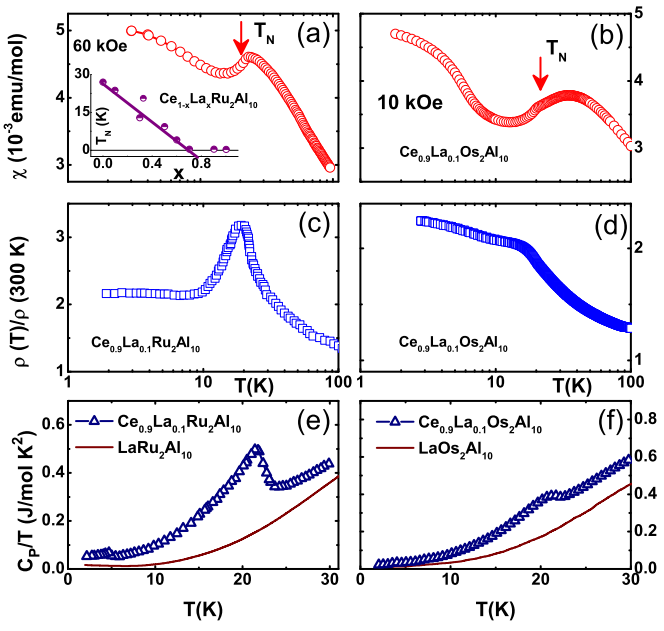

FIG. 2. (Color online) (a) and (b) Temperature dependence of dc magnetic susceptibility $\chi(T)$ $Ce_{1-x}La_xT_2Al_{10}$ with $x = 0.1$ (T = Ru and Os). Inset shows the variation of T_N with La composition for $Ce_{1-x}La_xRu_2Al_{10}$ [29]. (c) and (d) Semilogarithmic plot of electrical resistivity vs temperature. (e) and (f) Temperature variation of specific heat C_P divided by temperature for $Ce_{1-x}La_xT_2Al_{10}$ (T = Ru and Os) (open symbol) with nonmagnetic counterpart $LaRu_2Al_{10}$ and $LaOs_2Al_{10}$ (solid line).

a kink near 21.7 K. The former is due to an opening of the spin gap, while the latter is due to the onset of the antiferromagnetic ordering. A very similar behavior of $\chi(T)$ [10] with a broad maximum at 31 K (due to spin gap formation) above $T_N = 23$ K is observed for $CeRu_{1.96}Re_{0.06}Al_{10}$. The inverse magnetic susceptibilities of $Ce_{0.9}La_{0.1}Ru_2Al_{10}$ and $Ce_{0.9}La_{0.1}Os_2Al_{10}$ exhibit Curie-Weiss behavior between 50 and 300 K. A linear least-squares fit to the data yields an effective magnetic moment $\mu_{\rm eff} = 2.12\,\mu_B$ and a paramagnetic Curie temperature $\theta_p = -95$ K for $Ce_{0.9}La_{0.1}Ru_2Al_{10}$ and $\mu_{\rm eff} = 2.58\ \mu_B$ and $\theta_p = -175$ K for $Ce_{0.9}La_{0.1}Os_2Al_{10}$. The value of the magnetic moment suggests that the Ce atoms are in their normal Ce^{3+} valence state in both compounds. The negative value of θ_p is in agreement with AFM ordering, a negative sign for the exchange interactions, and/or the presence of the Kondo effect. The larger negative value of θ_p of $Ce_{0.9}La_{0.1}Os_2Al_{10}$ compared to that of $Ce_{0.9}La_{0.1}Ru_2Al_{10}$ suggests a stronger hybridization in the former. The inset in Fig. 2(a) shows the La composition dependence of T_N of $Ce_{1-x}La_xRu_2Al_{10}$, which reveals that T_N decreases almost linearly and becomes zero near $x \geqslant 0.7$ [12,29]. In this critical region of compositions the heat capacity exhibits a rise at low temperature suggesting the presence of non-Fermi-liquid (NFL) behavior close to a quantum critical point (QCP) [29].

Figures 2(c) and 2(d) show the electrical resistivity $\rho(T)$ of $Ce_{0.9}La_{0.1}Ru_2Al_{10}$ and $Ce_{0.9}La_{0.1}Os_2Al_{10}$, respectively. At high temperature $\rho(T)$ of both samples increases with decreasing temperature up to T_N. Then $\rho(T)$ of $Ce_{0.9}La_{0.1}Ru_2Al_{10}$ exhibits a peak near T_N and remains metallic at low temperature, while for $Ce_{0.9}La_{0.1}Os_2Al_{10}$ the $\rho(T)$ shows a slope change at T_N, but still increases with further decrease in the temperature down to 2 K. This contrasting behavior of the low temperature resistivity is similar to that observed in the undoped compounds [14,15]. It is interesting to note that the resistivity of slightly electron (8% Ir) and hole (2% Re) doped $CeOs_2Al_{10}$ exhibits metallic behavior in all direction below T_N [24].

Figures 2(e) and 2(f) show the heat capacity divided by temperature C_P/T vs T of $Ce_{0.9}La_{0.1}Ru_2Al_{10}$ and $Ce_{0.9}La_{0.1}Os_2Al_{10}$ along with their respective nonmagnetic phonon reference compounds $LaRu_2Al_{10}$ and $LaOs_2Al_{10}$. The heat capacity of $Ce_{0.9}La_{0.1}Ru_2Al_{10}$ exhibits a λ-type anomaly near T_N, while the anomaly is considerably suppressed in $Ce_{0.9}La_{0.1}Os_2Al_{10}$. A rapid suppression of the heat capacity anomaly near T_N was also observed both in $CeRu_{1.94}Re_{0.06}Al_{10}$ and $CeOs_{1.96}Re_{0.04}Al_{10}$ [11,24]. By fitting the high temperature heat capacity data above T_N to $C_P/T = \gamma + \beta T^2$, we have estimated the Sommerfeld coefficient $\gamma = 0.125\,\mathrm{J/mol\,K^2}$ and $\beta = 3.5 \times 10^{-4}\,\mathrm{J/mol\,K^4}$ for $Ce_{0.9}La_{0.1}Ru_2Al_{10}$ and $\gamma = 0.133\,\mathrm{J/mol\,K^2}$ and $\beta = 5.1 \times 10^{-4}\,\mathrm{J/mol\,K^4}$ for $Ce_{0.9}La_{0.1}Os_2Al_{10}$. The observed values of γ are smaller than those observed for undoped compounds, $\gamma = 0.2\ \mathrm{J/mol\,K^2}$ for $CeRu_2Al_{10}$ and $\gamma = 0.541\ \mathrm{J/mol\,K^2}$ for $CeOs_2Al_{10}$, indicating that heavy fermion behavior is suppressed by the La doping. From the value of $\beta = (12\pi^4/5)\ (nN_Ak_B/\Theta_D^3)$, where N_A and k_B have the usual meaning, and $n = 13$ is the number of atoms per f.u., we estimated the Debye temperature to $\Theta_D = 416$ and 367 K for $Ce_{0.9}La_{0.1}Ru_2Al_{10}$ and $Ce_{0.9}La_{0.1}Os_2Al_{10}$, respectively.

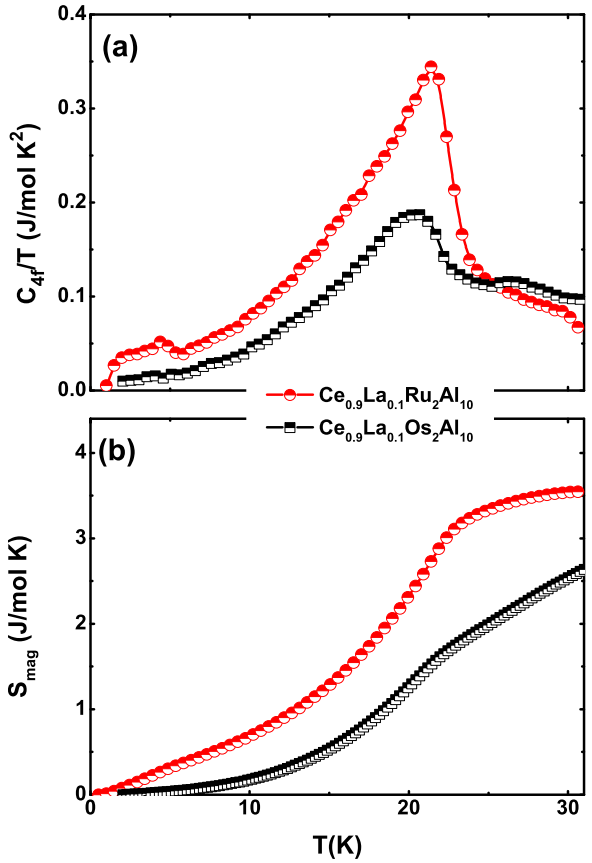

FIG. 3. (Color online) (a) Temperature variation of magnetic specific heat C_{4f} for $Ce_{0.9}La_{0.1}T_2Al_{10}$ (T = Ru, Os). (b) Calculated magnetic entropy as a function of temperature.

Figure 3(a) shows the magnetic heat capacity variation with temperature for $Ce_{0.9}La_{0.1}Ru_2Al_{10}$ and $Ce_{0.9}La_{0.1}Os_2Al_{10}$. The value of magnetic entropy S_{mag} [Fig. 3(b)] at 30 K is 3.5 J/mol K for $Ce_{0.9}La_{0.1}Ru_2Al_{10}$ and 2.65 J/mol K for $Ce_{0.9}La_{0.1}Os_2Al_{10}$, which is much smaller than $R\ln(2) = 5.76$ J/mol K. The reduced magnetic entropy can be explained on the basis of the Kondo effect. We also estimated the gap in the spin wave by fitting $C_{mag(T)}$ data below T_N, and we find energy gap values 50 K for $Ce_{0.9}La_{0.1}Ru_2Al_{10}$ and 60 K for $Ce_{0.9}La_{0.1}Os_2Al_{10}$, whose values are approximately half of those reported for the undoped compounds [8]. The weak anomaly seen in the magnetic heat capacity data of the $Ce_{0.9}La_{0.1}Ru_2Al_{10}$ compound below 5 K should be attributed to a contribution from an impurity, the amount of which should according to the neutron diffraction data be less than 5%. This anomaly was not seen in the heat capacity data of Tanida *et al.* [33].

IV. NEUTRON DIFFRACTION

Figures 1(a) and 1(b) show the ND patterns for $Ce_{0.9}La_{0.1}Ru_2Al_{10}$ and $Ce_{0.9}La_{0.1}Os_2Al_{10}$, collected at 300 K on the D2B instrument in the high resolution mode. Both patterns are consistent with the $Cmcm$ symmetry and can be satisfactorily fitted with the structural model proposed earlier [1]. The structural parameters for both samples are listed in Table I. A comparison of the lattice parameters of the doped compounds with the parent ones shows that 10% La doping in $CeRu_2Al_{10}$ results in a volume expansion of 0.14%, while 10% La doping in $CeOs_2Al_{10}$ increases the volume by 0.09%. This can be compared to the volume contraction of 0.10% observed in 3% Re-doped (or hole-doped) $CeRu_2Al_{10}$, where the ordered state moment of 0.20 μ_B is along the b axis. It is generally agreed that hole doping in both $CeRu_2Al_{10}$ and $CeOs_2Al_{10}$ increases the hybridization [10,25].

TABLE I. Lattice parameters of $Ce_{1-x}La_xT_2Al_{10}$ (T = Ru, Os) for $x = 0.1$ refined from the neutron diffraction data collected at 300 K in the orthorhombic $Cmcm$ space group.

Compounds	a (Å)	b (Å)	c (Å)	V (Å)
$CeRu_2Al_{10}$	9.1246	10.2806	9.1878	861.9 [34]
$Ce_{0.9}La_{0.1}Ru_2Al_{10}$	9.1298	10.2845	9.1928	863.1
$CeOs_2Al_{10}$	9.138	10.2662	9.1694	861.7 [3]
$Ce_{0.9}La_{0.1}Os_2Al_{10}$	9.1412	10.2668	9.1898	862.5

To investigate the magnetic structure, we carried out ND measurements on the D20 instrument at 1.5 and 35 K (12 h each temperature) on $Ce_{0.9}La_{0.1}Ru_2Al_{10}$ and $Ce_{0.9}La_{0.1}Os_2Al_{10}$. At 1.5 K we observed very weak magnetic Bragg peaks at scattering angles away from the nuclear Bragg peaks, which confirmed the long-range AFM ordering of the Ce moment at 1.5 K in both compounds. To see the magnetic Bragg peaks clearly, we plotted the difference between the 1.5 and 35 K data for both compounds, which are shown in Fig. 4, along with their 3% Re-doped counterparts (see Refs [10,25] for details of the ND experiment of these materials). The important observation is the qualitatively similar diffraction patterns between the La- and Re-doped compositions. The absence of the magnetic (0, 1, 0) peak near 10.3 Å in both $Ce_{0.9}La_{0.1}Ru_2Al_{10}$ and $CeRu_{1.94}Re_{0.06}Al_{10}$ indicates the ordered moments to be along the b axis, in contrast with along the c axis in the parent $CeRu_2Al_{10}$ compound as well as in the $Ce(Ru_{1x}Fe_x)_2Al_{10}$ series [10]. The conclusion about the b-axis moment direction comes directly from the fact that the magnetic neutron diffraction intensity is proportional to the square of the ordered moment component perpendicular to the scattering vector. On the other hand, in $Ce_{0.9}La_{0.1}Os_2Al_{10}$ several magnetic Bragg peaks were observed including the (0, 1, 0) one and the relative intensities of these peaks are very similar to those observed in $CeRu_2Al_{10}$, indicating that the moments are probably along the c axis. In spite of the different moment directions, all the observed magnetic Bragg peaks in $Ce_{0.9}La_{0.1}Ru_2Al_{10}$ and $Ce_{0.9}La_{0.1}Os_2Al_{10}$ can be indexed based on the same propagation vector $k = (1,0,0)$, which is identical to that found in pure $CeRu_2Al_{10}$ [4]. It is to be noted that the propagation vector $k = (0,1,0)$ proposed for $CeOs_2Al_{10}$ is equivalent to $k = (1,0,0)$ as they are both related by the allowed ($h + k$ even) reciprocal translation $G = (-1,1,0)$.

In the qualitative refinement of the magnetic structures, we employed a method whereby combinations of axial vectors localized on the 4c(Ce) site (as Ce is only the magnetic atom) and transforming as basis functions of the irreducible representations of the wave vector group are systematically tested. The symmetry analysis yields that the reducible

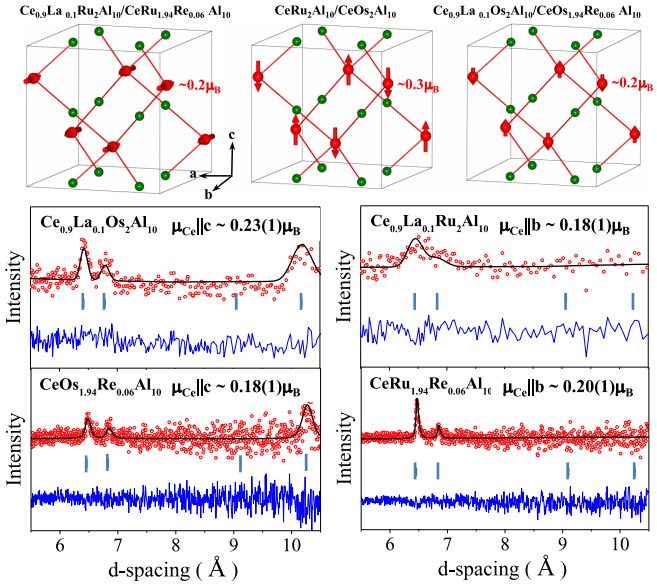

FIG. 4. (Color online) Rietveld refinements of the magnetic intensity of $Ce_{1-x}La_xT_2Al_{10}$ (T = Ru, Os) along with $Ce(Ru/Os_{1-x}Re_x)_2Al_{10}$ ($x = 0.03$) obtained as a difference between the diffraction patterns collected at 1.5 and 35 K. The circle symbols (red) and solid line represent the experimental and calculated intensities, respectively, and the line below (blue) is the difference between them. Tick marks indicate the positions of Bragg peaks for the magnetic scattering with the $k = (1,0,0)$ propagation vector. The upper panel shows the magnetic structures of the La-doped (found in this paper), $Ce(Ru/Os_{1-x}Re_x)_2Al_{10}$ ($x = 0.03$), and CeT_2Al_{10} (T = Ru and Os) samples. For clarity, only Ce and Ru/Re atoms are shown (top).

magnetic representation is decomposed into six one-dimensional representations, labeled Y_i^+ ($i = 2, 3, 4$) and Y_i ($i = 1, 2, 3$). The Y_i^+ representations result in a ferromagnetic (FM) alignment of the Ce moments within the primitive unit cell, along different crystallographic directions. On the other hand, Y_i^- transform Ce moments which are AFM coupled within the primitive unit cell. We refined the difference data (1.5–35 K) using the three AFM structures (with the moments along the a, b, and c axes) given by Y_i^- representations. The best fit to the data was obtained with a Ce ordered state moment of 0.18(2) μ_B AFM coupled along the b axis for $Ce_{0.9}La_{0.1}Ru_2Al_{10}$ (see Fig. 4, where the magnetic unit cells are shown), while an ordered moment of 0.23(1) μ_B along the c axis was obtained for $Ce_{0.9}La_{0.1}Os_2Al_{10}$.

It is interesting to compare these values of the ordered state moments with those found in the undoped systems, 0.34(2) μ_B for $CeRu_2Al_{10}$ and 0.29(2) μ_B for $CeOs_2Al_{10}$, both along the c axis [10,11]. This comparison shows a reduction of the ordered moment in 10% La-doped systems, which might be due to a change in the Ce valence with La doping as proposed in Ref. [31]. The different directions of the ordered state moment in 10% La-doped $CeRu_2Al_{10}$ and $CeOs_2Al_{10}$ is a surprising observation and can be only explained by assuming a different degree of hybridization (weak in the former material). This means that 10% La-doped $CeOs_2Al_{10}$ sees anisotropic exchange interactions which are still similar to those in the undoped compound preserving hence the moment direction. It should be possible to change the moment direction as well in La-doped $CeOs_2Al_{10}$ to the b axis by increasing the La content up to 50% in $CeOs_2Al_{10}$. However, the absolute value of the moment would certainly reduce further with increased doping, making its experimental detection difficult. The question remains why—despite having a smaller hybridization—the ordered moment in $Ce_{0.9}La_{0.1}Ru_2Al_{10}$ is smaller in comparison to that found in $Ce_{0.9}La_{0.1}Os_2Al_{10}$. It is to be noted that the estimated CEF moment for $CeRu_2Al_{10}$ is $\mu_{\rm CEF}^{a,b,c} = (1.44, 0.19, 0.38)\ \mu_B$ [17] and for $CeOs_2Al_{10}$ is $\mu_{\rm CEF}^{a,b,c} = (1.35, 0.27, 0.30)\ \mu_B$ [49]. These results suggest that the small value of the b-axis moment can be explained on the basis of the CEF effect, but the origin of the direction of the moment remains to be understood.

V. INELASTIC NEUTRON SCATTERING STUDY

With the dramatic and contrasting changes observed in the moment direction and its absolute value in 10% La-doped $CeRu_2Al_{10}$ and $CeOs_2Al_{10}$, it would be interesting to investigate directly the spin gap formation in these compounds using INS. Furthermore, Kawabata *et al.* [24] reported that the suppression of T_N is well correlated with the gap energy Δ as a function of electron (Ir) and hole (Re) doping and they conclude that the presence of the hybridization gap is indispensable for the AFM order at unusually high T_N in $CeOs_2Al_{10}$. Thus the information on the spin gap energy scale in $Ce_{0.9}La_{0.1}Ru_2Al_{10}$ and $Ce_{0.9}La_{0.1}Os_2Al_{10}$ is very important. Therefore, we briefly report the INS spectra, which give direct information of the spin gap energy, below and above T_N of 10% La-doped samples and undoped samples in this section. A detailed report on the INS investigations on CeT_2Al_{10} (T = Fe, Ru, and Os) compounds can be found in Ref. [3].

Figure 5 displays the INS spectra of 10% La-doped compounds with that of undoped compounds at two temperatures at

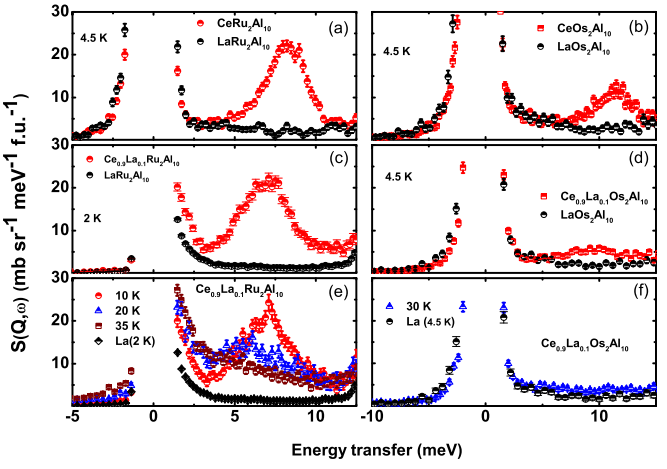

FIG. 5. (Color online) Q-integrated ($0 \leqslant Q \leqslant 2.5$ Å) intensity versus energy transfer of (a) and (b) CeT_2Al_{10} (T = Ru and Os) measured on the MARI spectrometer (c)–(f) $Ce_{0.9}La_{0.1}Ru_2Al_{10}$ and $Ce_{0.9}La_{0.1}Os_2Al_{10}$ measured on the IN4 spectrometer along with the nonmagnetic phonon reference compounds LaT_2Al_{10} (T = Ru and Os) (red half-filled circles), measured with respective incident energy of $E_i = 20$ meV. For IN4 we have made cuts in scattering angle between 13° and 43°.

low-Q measured on the MARI and IN4 spectrometers. There is a clear magnetic excitation centered around 7 and 10 meV in $Ce_{0.9}La_{0.1}Ru_2Al_{10}$ and $Ce_{0.9}La_{0.1}Os_2Al_{10}$, respectively, which may be compared to the 8 and 11 meV excitations found in the parent compounds, respectively [3,10,11]. The value of the peak position can be taken as a measure of the spin gap energy in these compounds. These results show that in both 10% La-doped systems, despite the moment direction being different and the ordered state moments being reduced, the spin gap energy scale remains unchanged. On the other hand, the intensity of the spin gap does not change much in $Ce_{0.9}La_{0.1}Ru_2Al_{10}$, while a dramatic reduction in the intensity of the spin gap is observed in $Ce_{0.9}La_{0.1}Os_2Al_{10}$. An interesting observation is the existence of a clear low energy response at low Q in $Ce_{0.9}La_{0.1}Ru_2Al_{10}$ at 2 K. This signal is not observed in the nonmagnetic phonon reference compound $LaRu_2Al_{10}$, which confirms its magnetic origin. Furthermore, the high resolution INS study on $CeRu_2Al_{10}$ by Robert *et al.* [21] did not reveal any clear sign of the low energy or quasielastic excitation at 11 K. This reveals that the low energy excitation in $Ce_{0.9}La_{0.1}Ru_2Al_{10}$ has some relation with changes in the moment direction from the c axis to the b axis. It is an open question whether this could be zero frequency mode observed in several magnetically ordered heavy fermion systems along with the spin waves below T_N for examples $CePt_3Si$, $CePd_2Si_2$, and $CeIn_3$ [38–40]. The coexistence of low-energy or quasielastic excitations and spin gap/spin waves indicates that Kondo spin fluctuations or longitudinal fluctuations are present with spin waves below T_N. The spin waves are transverse excitations and hence the presence of quasielastic excitations suggests the change in the nature of magnetic exchanges with La doping in $Ce_{0.9}La_{0.1}Ru_2Al_{10}$. This study will provide a starting point for the future single crystals work on spin waves measurements for the La-doped system as well as help the development of correct theoretical models to understand the complex magnetism in CeT_2Al_{10} (T = Ru and Os). On the other hand, within the resolution of MARI experiment, we could not see any clear sign of low energy excitation at 4.5 K in $Ce_{0.9}La_{0.1}Os_2Al_{10}$ as well as the absence of this excitation in $CeOs_2Al_{10}$ from the high resolution INS study [3].

Now we discuss the temperature dependence of the spin gap excitation. For $Ce_{0.9}La_{0.1}Ru_2Al_{10}$ with increasing temperature to 10 K no dramatic changes were observed in the spectra, but at 20 K the spin gap energy decreases to 5.5 meV and its width increases to 1.26 meV. Further increase in the temperature to 25 K (same response at 30 K), the inelastic response continues to broaden. The data show two components, a low energy/quasielastic component with narrow linewidth and a second, distinctly broader component. The Q-dependent integrated intensity of $Ce_{0.9}La_{0.1}Ru_2Al_{10}$ between 5 and 8 meV at 2 K nearly follows the Ce^{3+} magnetic form factor squared [$F^2(Q)$, figure not shown], very similar to that observed in pure $CeRu_2Al_{10}$ [6]. The observed single ion type response of $Ce_{0.9}La_{0.1}Ru_2Al_{10}$ in the magnetic ordered state could be due to the fact that the observed spin wave scattering intensity in $CeRu_2Al_{10}$ single crystal is stronger near the zone boundary and considering the presence of powder averaging effect could give single-ion type behavior. It is to be noted that the single-ion type response is also observed in the inelastic response of the spin gap system $CeRu_4Sb_{12}$, which does not exhibit any long-range magnetic ordering down to 50 mK [41]. On the other hand, the deviation from a single-ion response is observed in the spin gap system $CeFe_4Sb_{12}$, where it was proposed that the intersite interactions between Ce and Fe are playing an important role [42]. As the spin gaps in $CeOs_2Al_{10}$ and $CeRu_2Al_{10}$ open up below (or just above) T_N one would expect that the spin gap energy and its intensity would be strongly Q dependent, but this is not the case. Furthermore, with increasing temperature to 30 K the response of $Ce_{0.9}La_{0.1}Os_2Al_{10}$ also becomes very broad and intensity decreases considerably [Fig. 5(f)] compared with 4.5 K.

VI. MUON SPIN RELAXATION

Figures 6(a)–6(f) shows the zero-field (ZF) μSR spectra at various temperatures of $Ce_{1-x}La_xRu_2Al_{10}$ ($x = 0, 0.3, 0.5,$

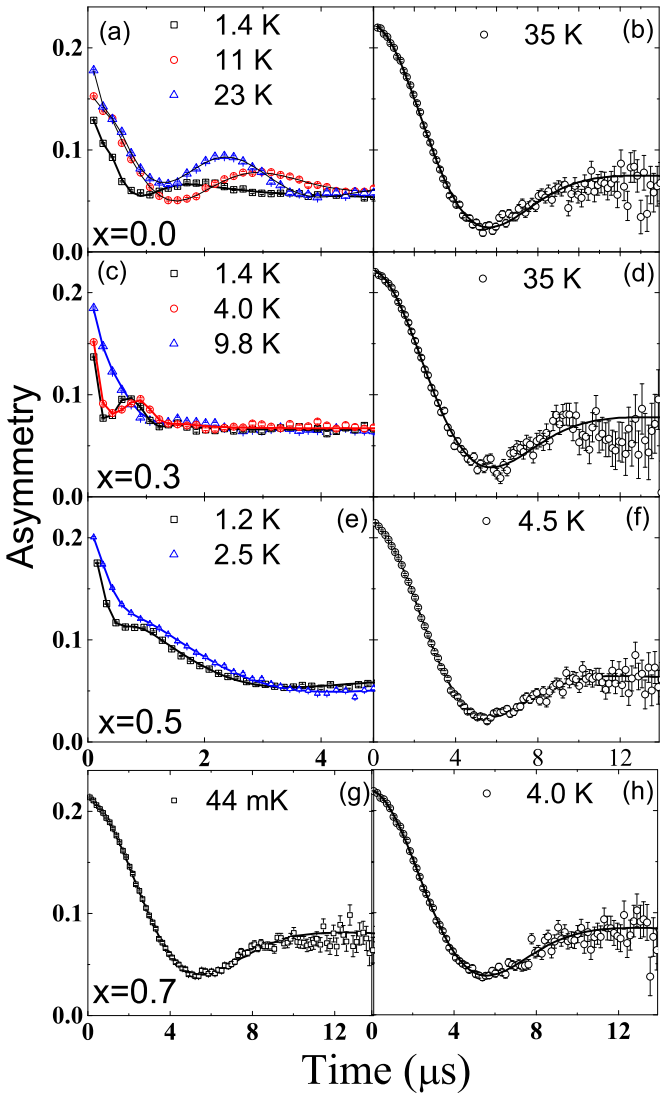

FIG. 6. (Color online) The time evolution of the muon spin relaxation in $Ce_{1-x}La_xRu_2Al_{10}$ for various temperatures (above and below T_N) in zero field. The solid line is a least-squares fit [using Eq. (1) (above T_N) and Eq. (2) (below T_N)] to the data as described in the text.

and 0.7). It is interesting to see the dramatic change in the time evolution of the μSR spectra with temperature for all compositions, except for $x = 0.7$. At 35 K (or 4.5 K) we observe a strong damping at shorter time, and the recovery at longer times for all compositions, which is a typical muon response to nuclear moment, known as the Kubo-Toyabe [43], arising due to a static distribution of the nuclear dipole moment. Here it arises from the La (stable isotope ^{138}La, $I = 5$, 0.09% abundance and ^{139}La, $I = 7/2$, 99.91% abundance), Ru (stable isotope ^{99}Ru, $I = 5/2$, 12.76% abundance, ^{101}Ru, $I = 5/2$, 17.06% abundance), and Al ($I = 5/2$) nuclear moment contributions ($I = 0$ for Ce, i.e., zero contribution). Above T_N the μSR spectra of all compounds ($x = 0$ to 0.7) can all be described by the following equation (see Fig. 6, right-hand figures):

$$G_z(t) = A_0\left\{\tfrac{1}{3} + \tfrac{2}{3}[1-(\sigma t)^2]e^{(-\sigma t)^2/2}\right\}e^{-\lambda t} + A_{\rm bg}, \quad (1)$$

where A_0 is the initial asymmetry, σ/γ_μ is the local field distribution, $\gamma_\mu = 13.55$ MHz/T is the gyromagnetic ratio of the muon, λ is the electronic relaxation rate arising from electronic moments, and $A_{\rm bg}$ is a constant background. It is assumed that the electronic moments give an entirely independent muon spin relaxation channel in real time. The value of σ was found to be 0.32(3) μs^{-1} for all compositions from fitting the spectra at high temperature (35 or 4.5/4 K) to Eq. (3), which suggests that muon stopping sites are the same for all compositions. From a simple electrostatic potential calculation of $CeRu_2Al_{10}$ Kambe *et al.* [44] have proposed a muon stopping site at 4*a* (0,0,0), while Khalyavin *et al.* [5] proposed a muon stopping site at 4*c* (0.5,0,0.25) (using electrostatic calculation of $CeOs_2Al_{10}$). Furthermore, the density functional theoretical (DFT) calculation of muon stopping sites in $Ce(Ru_{1-x}Rh_x)_2Al_{10}$ [45] supports both muon sites equally possible as they are located at local minimum positions of the electrostatic potential. Furthermore, the DFT calculation revealed that the muon stopping site (or position) estimated from the potential calculation does not change much with Rh doping [46] as there are no big changes in the potential around the suggested muon sites.

Now we discuss the muon spectra at low temperatures. As shown in the left side of Fig. 6, μSR spectra of $x = 0$, 0.3, and 0.5 exhibit a clear sign of coherent frequency oscillations confirming the long-range magnetic ordering of the Ce moment. On the other hand, μSR spectra of $x = 0.7$ at 44 mK reveal the same behavior as that observed at 4.0 K, indicates the nonmagnetic (or paramagnetic) ground state. The result is in agreement with the proposed phase diagram T_N vs x (La concentration), reveals $T_N \approx 0$ K for $x \geqslant 0.6$ [see the inset in Fig. 2(a)]. For the other compositions, the spectra below T_N are best described by two oscillatory terms and an exponential decay, as given by the following equation:

$$G_z(t) = \sum_{i=1}^{2} A_i \cos(\omega_i t + \phi)e^{-(\sigma t)^2/2} + A_3 e^{-\lambda t} + A_{\rm bg}, \quad (2)$$

where $\omega = \gamma_\mu H_{\rm int}$ is the muon precession frequency ($H_{\rm int}$ is the internal field at the muon site) and ϕ is the phase. In Fig. 7 (left) we have plotted the internal field (or muon precession frequency) at the muon site as a function of temperature. This shows that the two internal fields (or frequencies) appear just

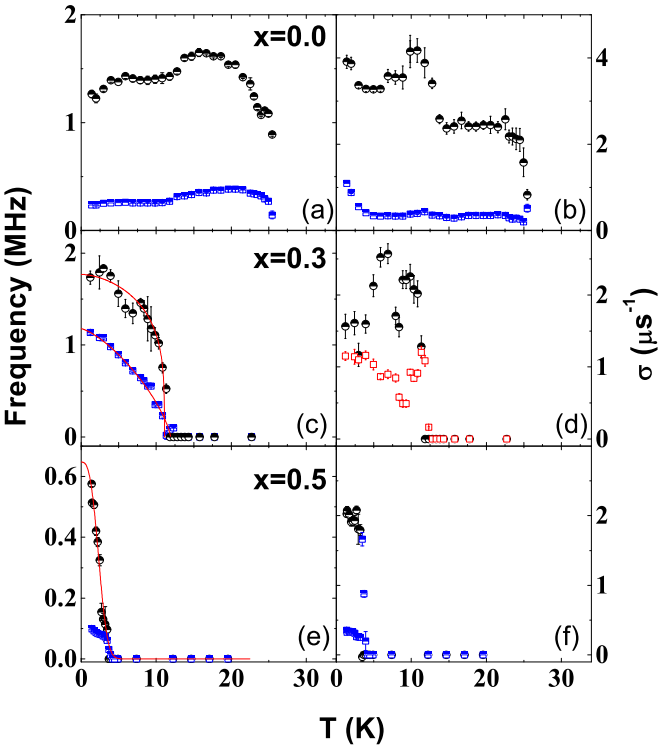

FIG. 7. (Color online) The temperature dependence of (a), (c), and (e) muon precession frequency/internal field at the muon site in $Ce_{1-x}La_xRu_2Al_{10}$. (b), (d), and (f) Depolarization rate σ. The solid line in (c) and (e) is fit to the data using Eq. (3) (see text).

below 27 K in $x = 0$, 12.5 K in $x = 0.3$, and 4.2 K in $x = 0.5$, showing a clear onset of bulk long-range magnetic order in agreement with T_N proposed in the inset of Fig. 2(a). Even though the heat capacity of $x = 0.3$ and 0.5 exhibits a very broad λ-type anomaly near T_N [47], the μSR shows a typical second order phase transition that can be explained by mean field behavior. Furthermore, the associated internal fields are found to be very small in agreement with a small ordered state magnetic moment of the Ce^{3+} ion observed in the ND for $x = 0$ and 0.1. The observed two values of internal fields can be explained on the basis of the dipole field calculation. It was found that Kambe's suggested positions correspond to the 4*a* sites, which had the lower field, and Khalyavin's suggested positions correspond to the 4*c* sites, which had the higher field. Furthermore, the temperature dependence of σ and the differences between the two values of σ also exhibit very similar behavior to that of the internal fields. The value of λ was found to be nearly temperature independent for all values of x.

Now examining the temperature dependence of the internal fields, we can see that there is a dip in the internal field (see Fig. 7 top left), which occurs around 15 K. Moreover, below 15 K the first and the second component of the depolarization rates also increase (Fig. 7 right). In principle, this could originate from various phenomena related to a change in distribution of internal fields, but a structural transition is a likely candidate in view of the structural instability reported on this system [2]. To find out the value of critical exponents and hence get more information on the nature of the magnetic

transition, the temperature dependence of the internal field was fitted [48]:

$$H_{\rm int}(T) = H_0\left[1 - \left(\frac{T}{T_N}\right)^{\alpha}\right]^{\beta}. \quad (3)$$

Fitting the temperature dependent internal field of $x = 0.3$ to Eq. (3) we obtained the value of the parameters for higher (and for lower) internal field: $T_N = 12.9(3)$ (same for both fields), $H_0 = 16.5(3)$ Oe [11.8(7) Oe], $\alpha = 1.65(6)$ [1.42(4)], and $\beta = 0.81(3)$ [0.89(2)]. Fit for $x = 0.5$ data fitting higher field we obtained $T_N = 4.06(9)$, $H_0 = 9.6(20)$ Oe, $\alpha = 0.99(30)$, and $\beta = 1.2(12)$. It is to be noted that due to limited temperature range the fit to lower field did not converge. It is interesting to compare these values of the exponents with $\alpha = 1.47(2)$ and $\beta = 0.96$ observed in $CeRu_{1.94}Re_{0.06}Al_{10}$ [10]. The larger values of β compared to 0.5, expected from the mean field theory suggests that magnetic interactions are complex in nature.

Now we compare the results of our ND and μSR of $Ce_{0.9}La_{0.1}Ru_2Al_{10}$ with that of the hole-doped systems $Ce(Ru_{0.97}Re_{0.03})_2Al_{10}$ and $Ce(Os_{0.97}Re_{0.03})_2Al_{10}$. The ND study of $Ce(Ru_{0.97}Re_{0.03})_2Al_{10}$ shows that this compound orders AFM with a propagation vector $k = (1,0,0)$ and the ordered state moment is 0.20(1) μ_B along the b axis, in sharp contrast with the ordered moment of 0.34–0.42 μ_B along the c axis observed in $CeRu_2Al_{10}$ ($T_N = 27$ K) [25], which is very similar behavior observed in $Ce_{0.9}La_{0.1}Ru_2Al_{10}$. The μSR study on $Ce(Ru_{0.97}Re_{0.03})_2Al_{10}$ reveals the presence of one internal field (frequency) with value of 80 Oe at 1.2 K. The observed single frequency in $Ce(Ru_{0.97}Re_{0.03})_2Al_{10}$ can be explained by the dipolar field calculation with muon stopping site at $4c$. On the other hand, the μSR study on $Ce_{1-x}La_xRu_2Al_{10}$ ($x = 0$, 0.3, and 0.5) shows the presence of two frequencies.

Furthermore, $Ce(Os_{0.97}Re_{0.03})_2Al_{10}$ has been studied by μSR and ND measurements. A long-range AFM ordering of the Ce sublattice with a substantially reduced value of the magnetic moment 0.18(1) μ_B along the c axis (same direction as in the undoped system) has been found below $T_N = 21$ K. On the other hand, the electron doping (i.e., Ir and Rh) in $CeRu_2Al_{10}$ and (Ir) in $CeOs_2Al_{10}$ show a large ordered moment of $\approx$1 μ_B along the a axis. The obtained result reveals the crucial difference between electron- and hole-doping effects on the magnetic ordering in CeT_2Al_{10} (T = Ru and Os). The former suppresses the anisotropic c-f hybridization and promotes localized Ce moments controlled by single ion anisotropy. On the contrary, the latter increases the hybridization, keeping the dominant role of the anisotropic exchange on the direction of the moments and shifts the system towards a delocalized nonmagnetic state [26].

Finally, it should be pointed out that the obtained results pose a question about the role of the hybridization and the crystal field effects in the reduced moment nature of the magnetic ground state in the undoped CeT_2Al_{10} (T = Ru and Os). The behavior of the system under the hole doping, electron doping, and chemical pressure (positive by Y doping and negative by La doping) along with the applied hydrostatic pressure study points to the key role of the hybridization in the anisotropic character of the exchange interactions observed in the undoped compound as well. This also implies the hybridization effect on the moments reduction, attributed by Strigari *et al.* [17,49] to the crystal field effects implicitly.

VII. CONCLUSIONS

We have carried out a comprehensive study on $Ce_{0.9}La_{0.1}T_2Al_{10}$ (T = Ru and Os) using the complementary techniques of magnetization, resistivity, heat capacity, ND, INS, and μSR measurements to understand the unusual behavior of the magnetic moment direction and opening of a spin gap below T_N (Table II). The ND study is unambiguous in confirming the long-range AFM order in these compounds. More interestingly, our ND study shows a very small ordered moment of 0.18 μ_B along the b axis in $Ce_{0.9}La_{0.1}Ru_2Al_{10}$, but a moment of 0.23 μ_B along the c axis in $Ce_{0.9}La_{0.1}Os_2Al_{10}$. This contrasting behavior can be explained based on a different degree of hybridization, which is stronger in $CeOs_2Al_{10}$ than in $CeRu_2Al_{10}$. Furthermore, it should not be related to a purely chemical pressure effect as then both La-doped systems should have the same direction of the moment, either along the c or a axis. Our INS study of 10% La-doped samples with T = Ru and Os reveals the spin gap energy remains at 7 and 10 meV, respectively, as in the undoped samples. Interestingly the intensity of the spin gap decreases dramatically in La-doped $CeOs_2Al_{10}$ compound.

Furthermore, we also present μSR study on $Ce_{1-x}La_xRu_2Al_{10}$ ($x = 0$, 0.3, 0.5, and 0.7), which reveals the presence of two coherent frequency oscillations indicating a long-range AFM ground state in $x = 0$ to 0.5, but almost temperature independent Kubo-Toyabe response for $x = 0.7$. The absence of temperature dependent relaxation rate in $x = 0.7$, despite the logarithmic rise in the heat capacity, is an unusual behavior. One would expect that near a quantum phase transition, μSR will sense the presence of quantum fluctuations even in the paramagnetic NFL state. These μSR results are very similar to that observed in YFe_2Al_{10}, where, despite NFL behavior observed in the magnetic susceptibility and heat capacity, the μSR spectra [3] are independent of temperature down to mK. A major achievement of our work has been the finding of frequency oscillations in the μSR spectra up to $x = 0.5$, which establishes the onset of long-range magnetic AFM in the La-doped compounds

TABLE II. A list of samples studied $Ce_{1-x}La_xT_2Al_{10}$ (T = Ru, Os) for $x = 0$, 0.1, and their transitions temperatures (T_N = antiferromagnetic ordering temperature), ground state magnetic moment ($\mu_{\rm AF}$ per f.u.) value, and moment directions (μ_d) obtained from neutron diffraction study (* this work).

Compounds	T_N (K)	(μ_B)	μ_d $\mu_{\rm AF}$	Spin gap (meV)
$CeRu_2Al_{10}$	27.0	0.34(2)	c axis [3]	8.0
$Ce_{0.9}La_{0.1}Ru_2Al_{10}$	23.0	0.18(2)	b axis*	7.0
$CeOs_2Al_{10}$	28.5	0.29(2)	c axis [3]	11
$Ce_{0.9}La_{0.1}Os_2Al_{10}$	21.7	0.23(1)	c axis*	10

and the robust magnetic ordering in spite of the large and anisotropic c-f hybridization in this system. The temperature dependence of the μSR frequencies and muon depolarization rates of $x = 0$ follow an unusual behavior with further cooling of the sample below 18 K, pointing at the possibility of another phase transition below 15 K. On the other hand, the temperature dependence of the μSR frequencies and muon depolarization rates of $x = 0.3$ follows conventional behavior expected for a second order phase transition in the mean field theory.

ACKNOWLEDGMENTS

Some of us (D.T.A. and A.D.H.) would like to thank CMPC-STFC for financial support. The work at Hiroshima University was supported by KAKENHI (Grant No. 26400363) from JSPS, Japan. A.M.S. acknowledges financial support from ERC Advanced Grant 227378 QuantumPuzzle. A.B. would like to acknowledge FRC of University of Johannesburg, NRF of South Africa, and ISIS-STFC for funding support. We would like to thank P. Manuel, J. M. Mignot, and I. Watanabe for an interesting discussion.

[1] V. M. T. Thiede, T. Ebel, and W. Jeitschko, J. Mater. Chem. **8**, 125 (1998).

[2] A. M. Strydom, Physica B **404**, 2981 (2009).

[3] D. T. Adroja, A. D. Hillier, Y. Muro, T. Takabatake, A. M. Strydom, A. Bhattacharyya, A. Daoud-Aladin, and J. W. Taylor, Phys. Scr. **88**, 068505 (2013).

[4] Y. Muro, K. Motoya, Y. Saiga, and T. Takabatake, J. Phys. Soc. Jpn. **78**, 083707 (2009).

[5] D. D. Khalyavin, A. D. Hillier, D. T. Adroja, A. M. Strydom, P. Manuel, L. C. Chapon, P. Peratheepan, K. Knight, P. Deen, C. Ritter, Y. Muro, and T. Takabatake, Phys. Rev. B **82**, 100405(R) (2010).

[6] D. T. Adroja, A. D. Hillier, P. P. Deen, A. M. Strydom, Y. Muro, J. Kajino, W. A. Kockelmann, T. Takabatake, V. K. Anand, J. R. Stewart, and J. Taylor, Phys. Rev. B **82**, 104405 (2010).

[7] D. T. Adroja, A. D. Hillier, Y. Muro, J. Kajino, T. Takabatake, P. Peratheepan, A. M. Strydom, P. P. Deen, F. Demmel, J. R. Stewart, J. W. Taylor, R. I. Smith, S. Ramos, and M. A. Adams, Phys. Rev. B **87**, 224415 (2013).

[8] T. Nishioka, Y. Kawamura, T. Takesaka, R. Kobayashi, H. Kato, M. Matsumura, K. Kodama, K. Matsubayashi, and Y. Uwatoko, J. Phys. Soc. Jpn. **78**, 123705 (2009).

[9] Y. Muro, J. Kajino, K. Umeo, K. Nishimoto, R. Tamura, and T. Takabatake, Phys. Rev. B **81**, 214401 (2010).

[10] A. Bhattacharyya, D. D. Khalyavin, D. T. Adroja, A. M. Strydom, A. D. Hiller, P. Manuel, T. Takabatake, J. W. Taylor, and C. Ritter, Phys. Rev. B **90**, 174412 (2014).

[11] A. Bhattacharyya, D. T. Adroja, A. M. Strydom, J. Kawabata, T. Takabatake, A. D. Hillier, V. Garcia Sakai, J. W. Taylor, and R. I. Smith, Phys. Rev. B **90**, 174422 (2014).

[12] H. Tanida, D. Tanaka, M. Sera, C. Moriyoshi, Y. Kuroiwa, T. Nishioka, H. Kato, and M. Matsumura, J. Phys. Soc. Jpn. **79**, 043708 (2010).

[13] K. Hanzawa, J. Phys. Soc. Jpn. **79**, 043710 (2010).

[14] C. S. Lue, H. F. Liu, B. D. Ingale, J. N. Li, and Y. K. Kuo, Phys. Rev. B **85**, 245116 (2012).

[15] C. S. Lue, S. H. Yang, A. C. Abhyankar, Y. D. Hsu, H. T. Hong, and Y. K. Kuo, Phys. Rev. B **82**, 045111 (2010).

[16] K. Yutani, Y. Muro, J. Kajino, T. J. Sato, and T. Takabatake, J. Phys.: Conf. Ser. **391**, 012070 (2012).

[17] F. Strigari, T. Willers, Y. Muro, K. Yutani, T. Takabatake, Z. Hu, Y.-Y. Chin, S. Agrestini, H.-J. Lin, C. T. Chen, A. Tanaka, M. W. Haverkort, L. H. Tjeng, and A. Severing, Phys. Rev. B **86**, 081105(R) (2012).

[18] S. C. Chen and C. S. Lue, Phys. Rev. B **81**, 075113 (2010).

[19] H. Kato, R. Kobayashi, T. Takesaka, T. Nishioka, M. Matsumura, K. Kaneko, and N. Metoki, J. Phys. Soc. Jpn. **80**, 073701 (2011).

[20] J. M. Mignot, P. A. Alekseev, J. Robert, S. Petit, T. Nishioka, M. Matsumura, R. Kobayashi, H. Tanida, H. Nohara, and M. Sera, Phys. Rev. B **89**, 161103(R) (2014).

[21] J. Robert, J. M. Mignot, S. Petit, P. Steffens, T. Nishioka, R. Kobayashi, M. Matsumura, H. Tanida, D. Tanaka, and M. Sera, Phys. Rev. Lett. **109**, 267208 (2012).

[22] J. Robert, J. M. Mignot, G. André, T. Nishioka, R. Kobayashi, M. Matsumura, H. Tanida, D. Tanaka, and M. Sera, Phys. Rev. B **82**, 100404(R) (2010).

[23] D. T. Adroja *et al.* (unpublished).

[24] J. Kawabata, T. Takabatake, K. Umeo, and Y. Muro, Phys. Rev. B **89**, 094404 (2014).

[25] D. D. Khalyavin, D. T. Adroja, A. Bhattacharyya, A. D. Hillier, P. Manuel, A. M. Strydom, J. Kawabata, and T. Takabatake, Phys. Rev. B **89**, 064422 (2014).

[26] D. D. Khalyavin, D. T. Adroja, P. Manuel, J. Kawabata, K. Umeo, T. Takabatake, and A. M. Strydom, Phys. Rev. B **88**, 060403(R) (2013).

[27] A. Kondo, J. Wang, K. Kindo, Y. Ogane, T. Takesaka, Y. Kawamura, T. Nishioka, D. Tanaka, H. Tanida, and M. Sera, J. Phys. Soc. Jpn. **80**, SA047 (2011).

[28] R. Kobayashi, Y. Ogane, D. Hirai, T. Nishioka, M. Matsumura, Y. Kawamura, K. Matsubayashi, Y. Uwatoko, H. Tanida, and M. Sera, J. Phys. Soc. Jpn. **82**, 093702 (2013).

[29] P. Peratheepan, Thermal, electronic and magnetic properties of the cage-structured rare-earth system RT_2Al_{10} (R = rare earth and $T = d$-electron element), Ph.D. thesis, University of Johannesburg, South Africa, 2014, https://ujdigispace.uj.ac.za/bitstream/handle/10210/8858/Peratheepan,%20P%202013.pdf?sequence=1.

[30] H. Tanida, H. Nohara, M. Sera, T. Nishioka, M. Matsumura, and R. Kobayashi, Phys. Rev. B **90**, 165124 (2014).

[31] Y. Oogane, Y. Kawamura, T. Nishioka, H. Kato, M. Matsumura, Y. Yamamoto, K. Kodama, H. Tanida, and M. Sera, J. Phys.: Conf. Ser. **400**, 032073 (2012).

[32] Y. Zekko, Y. Yamamoto, H. Yamaoka, F. Tajima, T. Nishioka, F. Strigari, A. Severing, J. F. Lin, N. Hiraoka, H. Ishii, K.-D. Tsuei, and J. Mizuki, Phys. Rev. B **89**, 125108 (2014).

[33] H. Tanida, D. Tanaka, Y. Nonaka, S. Kobayashi, M. Sera, T. Nishioka, and M. Matsumura, Phys. Rev. B **88**, 045135 (2013).

[34] Y. Muro, K. Hida, T. Fukuhara, J. Kawabata, K. Yutani, and T. Takabatake, Proc. Int. Conf. Strongly Correlated Electron Systems (SCES2013) [JPS Conf. Proc. **3**, 012017 (2014)].
[35] J. Rodríguez-Carvajal, Physica B **192**, 55 (1993).
[36] A. S. Wills, Physica B **276-278**, 680 (2000); Z. Kristallogr. Suppl. **30**, 39 (2009). Program SARAh available at ftp://ftp.ill.fr/pub/dif/sarah.
[37] H. T. Stokes, D. M. Hatch, and B. J. Campbell, ISOTROPY, stokes.byu.edu/isotropy.html (2007).
[38] B. Fåk, S. Raymond, D. Braithwaite, G. Lapertot, and J. M. Mignot, Phys. Rev. B **78**, 184518 (2008).
[39] N. H. van Dijk, B. Fåk and T. Charvolin, P. Lejay, and J.-M. Mignot, Phys. Rev. B **61**, 8922 (2000).
[40] W. Knafo, S. Raymond, B. Fåk, G. Lapertot, P. C. Canfield, and J. Flouquet, J. Phys. Condens. Matter **15**, 3741 (2003).
[41] D. T. Adroja, J.-G. Park, K. A. McEwen, N. Takeda, M. Ishikawa, and J.-Y. So, Phys. Rev. B **68**, 094425 (2003).
[42] R. Viennois, L. Girard, L. C. Chapon, D. T. Adroja, R. I. Bewley, D. Ravot, P. S. Riseborough, and S. Paschen, Phys. Rev. B **76**, 174438 (2007).
[43] R. Kubo and T. Toyabe, in Magnetic Resonance and Relaxation, edited by R. Blinc (North-Holland, Amsterdam, 1966), p. 810; R. S. Hayano, Y. J. Uemura, J. Imazato, N. Nishida, T. Yamazaki, and R. Kubo, Phys. Rev. B **20**, 850 (1979).
[44] S. Kambe, H. Chudo, Y. Tokunaga, T. Koyama, H. Sakai, U. Ito, K. Ninomiya, W. Higemoto, T. Takesaka, T. Nishioka, and Y. Miyake, J. Phys. Soc. Jpn. **79**, 053708 (2010).
[45] N. Adam, E. Suprayoga, B. Adiperdana, H. Guo, H. Tanida, S. S. Mohd-Tajudin, R. Kobayashi, M. Sera, T. Nishioka, M. Matsumura, S. Sulaiman, M. I. Mohamed-Ibrahim, and I. Watanabe, J. Phys.: Conf. Ser. **551**, 012053 (2014).
[46] H. Guo, H. Tanida, R. Kobayashi, I. Kawasaki, M. Sera, T. Nishioka, M. Matsumura, I. Watanabe, and Z. Xu, Phys. Rev. B **88**, 115206 (2013).
[47] H. Tanida, D. Tanaka, M. Sera, T. Nishioka, and M. Matsumura, J. Phys. Soc. Jpn. **80**, SA023 (2011).
[48] A. Bhattacharyya, D. T. Adroja, A. M. Strydom, A. D. Hillier, J. W. Taylor, A. Thamizhavel, S. K. Dhar, W. A. Kockelmann, and B. D. Rainford, Phys. Rev. B **90**, 054405 (2014).
[49] F. Strigari, T. Willers, Y. Muro, K. Yutani, T. Takabatake, Z. Hu, S. Agrestini, C.-Y. Kuo, Y.-Y. Chin, H.-J. Lin, T. W. Pi, C. T. Chen, E. Weschke, E. Schierle, A. Tanaka, M. W. Haverkort, L. H. Tjeng, and A. Severing, Phys. Rev. B **87**, 125119 (2013).